PET-Based Human Dosimetry of the Dimeric $\alpha_v\beta_3$ Integrin Ligand ^{68}Ga-DOTA-E-[c(RGDfK)]$_2$, a Potential Tracer for Imaging Tumor Angiogenesis

Victoria López-Rodríguez[1], Carlos Galindo-Sarco[2], Francisco O. García-Pérez[3], Guillermina Ferro-Flores[4], Oscar Arrieta[5], and Miguel A. Ávila-Rodríguez[1]

[1]Unidad Radiofarmacia-Ciclotrón, Facultad de Medicina, Universidad Nacional Autónoma de México, Mexico City, Mexico; [2]Departamento de Radiología, Instituto Nacional de Cancerología, Mexico City, Mexico; [3]Departamento de Medicina Nuclear, Instituto Nacional de Cancerología, Mexico City, Mexico; [4]Gerencia de Aplicaciones Nucleares en la Salud, Instituto Nacional de Investigaciones Nucleares, Ocoyoacac, Mexico; and [5]Departamento de Oncología Médica, Instituto Nacional de Cancerología, Mexico City, Mexico

Peptides containing the Arg-Gly-Asp (RGD) sequence have high affinity for $\alpha_v\beta_3$ integrin receptors overexpressed in tumor cells. The objective of this research was to determine the biodistribution and estimate the radiation dose from ^{68}Ga-DOTA-E-[c(RGDfK)]$_2$ using whole-body PET scans in humans. **Methods:** Five healthy volunteers (2 women, 3 men; mean age ± SD, 37.2 ± 15.6 y; range, 28–65 y; mean weight, 79.2 ± 21.0 kg; range, 64–115 kg) were included. After intravenous injection of the tracer (198.3 ± 3.3 MBq), 3 successive whole-body (vertex to mid thigh) PET/CT scans at 3 time points (30, 60, and 120 min) were obtained on a 16-slice PET/CT scanner. The subjects did not void the bladder until the entire series of images was completed. Low-dose CT without contrast agent was used for anatomic localization and attenuation correction. OLINDA/EXM software was applied to calculate human radiation doses using the reference adult model. **Results:** The highest uptake was in the urinary bladder, followed by the liver, kidneys, and spleen, in descending order. The critical organ was the urinary bladder wall. The mean effective doses (all subjects, men and women) were 34.1 ± 4.9, 31.0 ± 2.4, and 20.9 ± 5.2 μSv/MBq for the no-voiding, 2.5-h-voiding, and 1-h-voiding models, respectively. **Conclusion:** Of particular interest in this research was the visualization of the choroid plexus and ventricular system, which seems to be a characteristic of RGD–dimeric peptides. Measured absorbed doses and effective doses are comparable to other previously reported RGD-based radiopharmaceuticals labeled with ^{68}Ga and ^{18}F. Therefore, ^{68}Ga-DOTA-E-[c(RGDfK)]$_2$ can safely be used for imaging integrin $\alpha_V\beta_3$ expression.

Key Words: ^{68}Ga-DOTA-E-[c(RGDfK)]$_2$; $\alpha_V\beta_3$ integrin receptors; angiogenesis; human dosimetry; RGD–dimeric peptides

J Nucl Med 2016; 57:404–409
DOI: 10.2967/jnumed.115.161653

The last few years have witnessed the development of a virtual revolution in PET molecular imaging, and radiolabeled receptor-binding peptides are emerging as powerful tools for imaging and therapy applications of tumors expressing peptide binding receptors (*1–3*). Somatostatin analogs have been in use the longest, have led to the accumulation of a vast amount of data, and have proven useful for the management of patients with neuroendocrine tumors (*4–8*). Several other peptide receptor–binding compounds have been synthesized within the past few years and are currently in various research stages—in vitro, in vivo, and preclinical studies—but have not yet been approved for clinical use (*9–11*). These new and rapidly expanding peptide-based radiopharmaceuticals deserve close attention.

It has been shown that peptides based on the RGD amino acid sequence have a high affinity and selectivity for $\alpha_V\beta_3$ integrin receptors (*12*). The $\alpha_V\beta_3$ integrins are transmembrane proteins that are preferentially expressed on proliferating endothelial cells but absent from quiescent endothelial cells (*13*). Integrins are overexpressed on newly formed blood vessels of actively growing tumors and are therefore potential targets for receptor-mediated tumor imaging and therapy when labeled with the proper radionuclide. Angiogenesis, the formation of new blood vessels from existing ones, is an essential process in solid tumors growing beyond 2–3 mm^3 since diffusion is no longer sufficient to supply the tissue with oxygen and nutrients. Integrins $\alpha_V\beta_3$ have been shown to play an important role in a series of pathologic processes including angiogenesis and tumor cell metastasis (*2,13–18*). Given the high affinity of RGD-based peptides for $\alpha_V\beta_3$ integrin receptors, a variety of cyclic RGD peptide conjugates have been used to target tumors overexpressing these receptors (*9–12,14–16,19,20*). However, it has been demonstrated that the dimeric conjugate is more suitable, for both imaging and therapeutic applications, than the monomeric conjugate. Li et al. showed that the dimeric and monomeric peptide had similar tumor-to-kidney ratios but that the dimer had higher tumor uptake and a prolonged retention time, making it more suitable than the monomer (*21*).

The choice of a radionuclide for PET-based molecular imaging applications depends on many parameters, including its physical half-life, decay profile, chemistry, and in vivo kinetics, as well as its availability and cost. In this regard, the availability of the ^{68}Ge/^{68}Ga generator is ideally suited for the demand for ^{68}Ga for clinical

Received Jul. 21, 2015; revision accepted Nov. 9, 2015.
For correspondence or reprints contact: Miguel A. Ávila-Rodríguez, Unidad Radiofarmacia-Ciclotrón, Facultad de Medicina, UNAM, Torre de Investigación, P.B. Ciudad Universitaria, Circ. Exterior, México, D.F., 04510, Mexico.
E-mail: avilarod@uwalumni.com
Published online Nov. 19, 2015.

applications in PET centers that lack an on-site cyclotron (*22–25*). ^{68}Ga is a positron emitter with a 68-min half-life and good characteristics for PET imaging (89% β^+, maximum β energy, 1.899 MeV). Additionally, the long half-life of ^{68}Ge (271 d) is attractive for cost-effectively operating the generator over a long period.

Recently, several publications have reported on various radiolabeled RGD-containing peptides with high affinity and selectivity for $\alpha_V\beta_3$ integrin receptors both in vitro and in vivo in animal models (*10,14–16*). Additionally, detailed biodistribution and measured radiation dosimetry in humans have been reported for ^{18}F-galactoRGD (*26*), ^{18}F-RGD-K5 (*27*), ^{68}Ga-NOTA-RGD (*28*), and ^{18}F-FPPRGD2 (*29*). Given the proven higher affinity of RGD–dimeric conjugates for $\alpha_V\beta_3$ integrin receptors (*17–20*), RGD–dimeric derivatives labeled with ^{99m}Tc (*30,31*) for SPECT and with ^{18}F (*29,32*) for PET have been evaluated in humans.

The aim of this research was to measure the human radiation dosimetry of a ^{68}Ga-labeled DOTA-conjugated RGD–dimeric peptide, E-[c(RGDfK)]$_2$, using biodistribution data obtained from whole-body PET/CT scans of healthy volunteers.

MATERIALS AND METHODS

Radiopharmaceutical Preparation

Ultrapure (>99.999% trace metal basis) HCl and NaOAc were purchased from Sigma-Aldrich. Cyclo(L-arginylglycyl-L-α-aspartyl-D-phenylalanyl-L-lysyl), 5,5′-[*N*-[[4,7,10-tris(carboxymethyl)-1,4,7,10-tetraazacyclododec-1-yl]acetyl]-L-glutamoyl]bis-(DOTA-E-[c(RGDfK)]$_2$) was obtained from ABX Advanced Biomedical Compounds. ^{68}Ga was obtained from a ^{68}Ge/^{68}Ga generator (Isotope Technologies Garching). The generator was eluted with 4 mL of 0.05 M HCl, and labeling was performed using a fractionation elution method. The first and last fractions of $^{68}GaCl_3$ (1.0 and 1.7 mL, respectively) were discharged, and only the second fraction (1.3 mL), containing approximately 80% of the activity, was used for labeling. Briefly, in a 1.5-mL Eppendorf tube containing 50 μg of DOTA-E-[c(RGDfK)]$_2$ and 165 μL of 0.5 M NaOAc were added 1.3 mL of freshly eluted $^{68}GaCl_3$ (~740 MBq). The reaction mixture (pH ~ 4.0) was kept at 95°C in a compact thermomixer (Eppendorf) at 300 rpm. The final product was diluted with 4 mL of physiologic saline solution and sterilized by being passed through a 0.22-μm syringe filter (Millex-GV). When needed, the final product was purified by solid-phase extraction using Oasis HLB cartridges (Waters). The structural formula of ^{68}Ga-DOTA-E-[c(RGDfK)]$_2$ is shown in Figure 1.

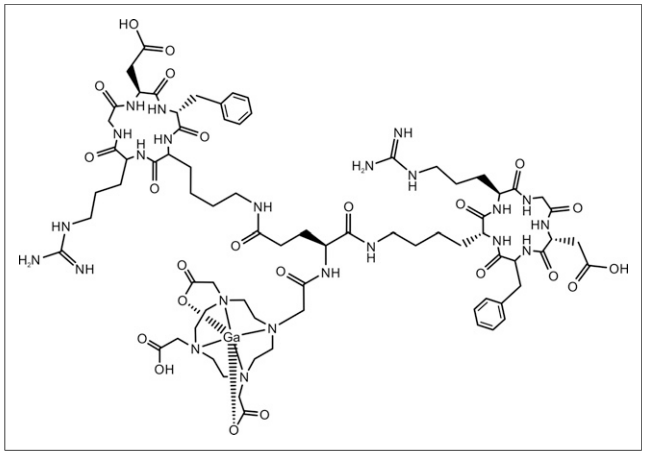

FIGURE 1. Structural formula of ^{68}Ga-DOTA-E-[c(RGDfK)]$_2$.

The radiochemical purity of ^{68}Ga-DOTA-E-[c(RGDfK)]$_2$ was determined by analytic high-performance liquid chromatography on a dual-pump Waters apparatus equipped with ultraviolet and radiation detectors. Analysis was performed using a Nova-Pak C18 column (3.9 × 150 mm; Waters) with a flow rate of 3 mL/min. The eluent components were A = 0.1N trifluoroacetic acid and B = CH_3CN, and the following gradient elution technique was adopted for separation: 0–1.5 min, 95% A + 5% B isocratic; 1.5–2.0 min, from 5% to 100% B in linear gradient; 2–3 min, 100% B; 3–4 min, from 100% to 5% B in linear gradient.

Human Subjects

Five healthy subjects (mean age ± SD, 37.2 ± 15.6 y; age range, 28–65 y; 3 men and 2 women) were included. Prescreening consisted of a detailed review of medical history and a physical examination. Subjects with evidence of clinical disease or a history of organ-removal surgery were excluded. The PET/CT scans were obtained at the National Institute of Cancer under the approval of the Bioethical Committee. Written informed consent was obtained from each subject. Mean (±SD) subject weight was 79.2 ± 21.0 kg (range, 64–115 kg).

PET/CT Acquisition

Imaging was performed on a Biograph 16 PET/CT scanner (Siemens Medical Solutions). To avoid biologic elimination, the subjects urinated before the examination and did not urinate again until after the entire series of images had been completed. Before administration of the tracer, a low-dose CT scan without contrast agent was acquired for anatomic localization and attenuation correction. The acquisition parameters of the helical CT scan were 120 kVp, 180 mAs, and 5-mm slice thickness. After intravenous injection of ^{68}Ga-DOTA-E-[c(RGDfK)]$_2$ (198.3 ± 3.3 MBq), 3 consecutive whole-body emission scans were acquired approximately 30, 60, and 120 min after injection, in close agreement with a previous publication on the dosimetry of ^{68}Ga-DOTATATE in humans (*8*). The whole-body PET scans were acquired from the vertex to mid thighs, at 2–3 min per bed position in 3-dimensional mode. To keep the x-ray dose as low as possible, the subjects remained motionless on the bed of the scanner until the entire series of emission scans had been completed so that the same CT scan could be used for the 3 emission scans. PET images were reconstructed using a 2-dimensional ordered-subset expectation maximization algorithm and were corrected for scatter, randoms, dead time, and decay. The resulting voxels were stored as units of Bq/mL.

Imaging Analysis

All PET/CT images were archived in DICOM format and were analyzed using OsiriX MD Imaging Software (Pixmeo SARL). The source organs were chosen from visually identifiable regions of the PET/CT images, including the thyroid, spleen, liver, kidneys, urinary bladder, choroid plexus, and ventricular system. Volumes of interest were drawn around the source organs and whole body onto each frame of the 3 scans. The total activity of each organ was determined by multiplying the mean activity concentration (Bq/mL or Bq/cm^3) by the CT-derived volume of interest, and the percentage of injected activity per organ was calculated as the ratio between the measured activity in the organ and activity in the whole-body scan acquired at the first time point (estimated to be about 80% because of omission of portions of the extremities). The activity, expressed as percentage injected dose, was plotted against time to obtain the time–activity curves of measured organs. The resulting time–activity curves were fitted to exponential equations, and the curves were extrapolated beyond the measured data points using the fitted equations.

Radiation Dosimetry Estimates

In this study, absorbed radiation doses and effective doses were calculated on the basis of the RADAR method (*33*) by entering the normalized number of disintegrations of each source organ into OLINDA/EXM software, version 1.1 (Vanderbilt University), using the standardized adult male and female models (*34*). The OLINDA/EXM kinetic analysis module was used to calculate the normalized number of disintegrations (time-integrated activity coefficient) of organs showing an exponential decrease, such as thyroid, spleen, liver, and kidneys. Organ volumes derived from CT were converted to mass using density values from publication 89 of the International Commission on Radiological Protection. The normalized number of disintegrations in the urinary bladder wall was calculated using the OLINDA/EXM dynamic bladder model (*35*) with no voiding and with 1- and 2.5-h bladder voiding intervals. Finally, the normalized number of disintegrations for the gastrointestinal tract was estimated using the gastrointestinal tract model (publication 30, International Commission on Radiological Protection) included in the OLINDA/EXM code and assuming an activity fraction of 0.05–0.07 entering the small intestine, as images revealed that 6.0% ± 0.8% of the total activity was excreted into the intestine at 30 min after injection. This model assumes that a fraction of injected activity enters the small intestine with no reabsorption.

Statistical Methods

Data are presented as mean ± SD unless otherwise stated.

RESULTS

The labeling yield was almost quantitative, with a radiochemical purity greater than 97% without the need for purification. The retention times for free $^{68}GaCl_3$ and ^{68}Ga-DOTA-E-[c(RGDfK)]$_2$ were 0.5 ± 0.1 and 2.5 ± 0.2 min, respectively. The content of the long-lived ^{68}Ge in the final product was less than 0.002% of the total radioactivity of ^{68}Ga, as measured by γ-spectroscopy using a high-purity germanium detector 48 h after the end of the radiolabeling synthesis.

The injection of 198.3 ± 3.3 MBq of ^{68}Ga-DOTA-E-[c(RGDfK)]$_2$ (17.7 ± 7.3 nmol of DOTA-E-[c(RGDfK)]$_2$) produced no observable adverse events or clinically detectable pharmacologic effects in any of the 5 subjects. Figure 2 shows the representative normal biodistribution of the radiotracer at 30, 60, and 120 min after injection, and Table 1 shows the biodistribution data for the 5 subjects, expressed as percentage injected activity per organ. Time–activity curves for the spleen, kidneys, liver, and urinary bladder are shown in Figure 3. The normalized number of disintegrations for the different organs in men and women is listed in Table 2, and the mean organ doses and effective doses are given in Table 3 for the different models used.

DISCUSSION

This study represents, to the best of our knowledge, the first-in-human biodistribution and radiation dosimetry measurements of a DOTA-conjugated RGD–dimeric peptide. The evaluated ^{68}Ga-DOTA-E-[c(RGDfK)]$_2$ revealed a biodistribution dominated by activity in the bladder, liver, kidneys, and spleen. The dosimetry calculations revealed the urinary bladder wall as the critical organ, with a mean (±SEM; all subjects, men and women) absorbed dose of 417 ± 71 μGy/MBq for the kinetic input model (no voiding). This dose decreased to 360 ± 66 and 172 ± 31 μGy/MBq for the 2.5- and 1-h-voiding models, respectively. On the other hand, the mean (±SEM) effective doses were 34.05 ± 4.85, 31.00 ± 2.37, and 20.85 ± 5.18 for the no-voiding, 2.5-h-voiding, and 1-h-voiding models, respectively. In general, the radiation doses were higher for women than men because of the smaller body and organ sizes of women. Additionally, the female gonads are inside the body instead of outside and receive a higher radiation dose given their proximity to organs such as the urinary bladder, liver, and kidneys, which are often important source organs. The small female sample size

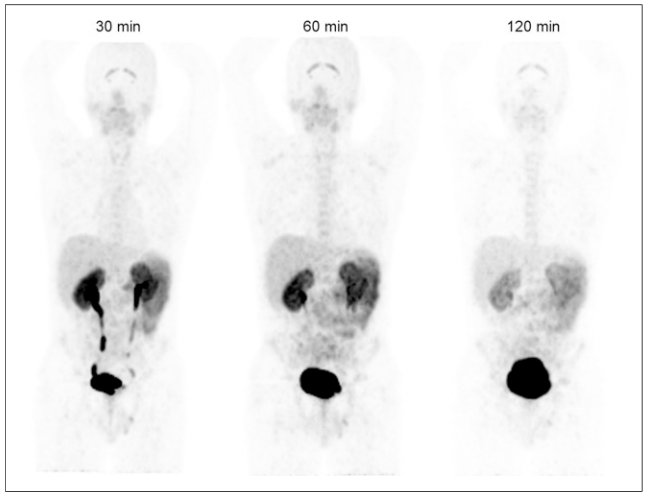

FIGURE 2. Typical biodistribution of ^{68}Ga-DOTA-E-[c(RGDfK)]$_2$ at 30, 60, and 120 min after injection.

TABLE 1
Biodistribution in Healthy Subjects after Intravenous Administration of ^{68}Ga-DOTA-E-[c(RGDfK)]$_2$

Tissue	0.5 h	1 h	2 h
Choroid plexus	0.0393 ± 0.0018	0.0350 ± 0.0014	0.0266 ± 0.0030
Thyroid	0.0504 ± 0.0051	0.0447 ± 0.0047	0.0342 ± 0.0015
Spleen	1.0058 ± 0.1374	0.9020 ± 0.1128	0.7578 ± 0.0615
Kidneys	2.4065 ± 0.2234	1.8632 ± 0.1883	1.3657 ± 0.0677
Liver	6.594 ± 0.5563	6.1797 ± 0.4814	5.5931 ± 0.4498
Urinary bladder	9.6152 ± 2.4242	16.5708 ± 2.4702	26.1134 ± 2.8535

Data are mean ± SD percentage injected dose per organ.

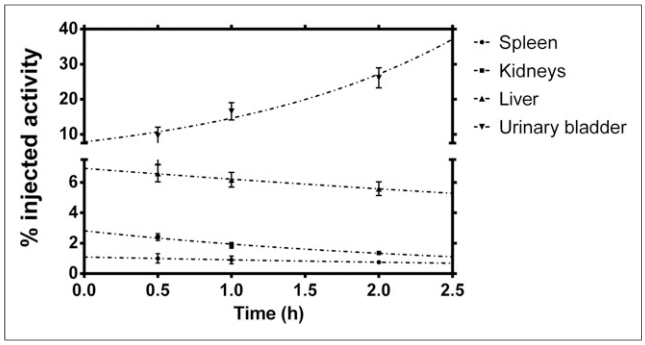

FIGURE 3. Time–activity curves of spleen, kidneys, liver, and urinary bladder.

could be a limitation, but considering that for diagnostic purposes the effective dose is most relevant, it is expected that the mean effective doses for most of the patients (all subjects, men and women) will be in the range reported in this study.

The absorbed and effective doses of other RDG-based PET radiopharmaceuticals recently reported in the literature are listed in Table 4. This table shows that the effective dose of ^{68}Ga-DOTA-E-[c(RGDfK)]$_2$ is comparable to the effective doses of other ^{68}Ga- and ^{18}F-labeled radiopharmaceuticals. For a typical 185-MBq administered activity of ^{68}Ga-DOTA-E-[c(RGDfK)]$_2$, the effective dose for the 1-h-voiding model is estimated to be 3.9 mSv, which is almost half the estimated 7 mSv in a typical whole-body PET scan with ^{18}F-FDG.

Of particular interest in this research was the observed uptake in the brain, specifically in the choroid plexus and ventricular system. Previous publications on the biodistribution and radiation dosimetry of radiopharmaceuticals that are based on RGD–dimeric peptides have reported such a finding (*29,32*); however, this uptake has not been observed with monomers of RGD. Other authors have reported the expression of a vast variety of integrin receptors in different structures of the adult brain, including the heterodimeric $\alpha_V\beta_3$ and its subunits α_V and β_3, which may explain this uptake (*36–38*). Prediction of the partition coefficient for the gallium-RGD monomer is CLogP = −1.8651 and for gallium-RGD dimer is CLogP = −1.7783 (ChemBioDraw Ultra program). The small difference between these values does not explain any possible ability of the dimer derivative to cross the blood–brain barrier. A clear choroid plexus visualization, as shown in Figure 4, has previously been reported in humans only for RGD–dimeric radiopeptides and

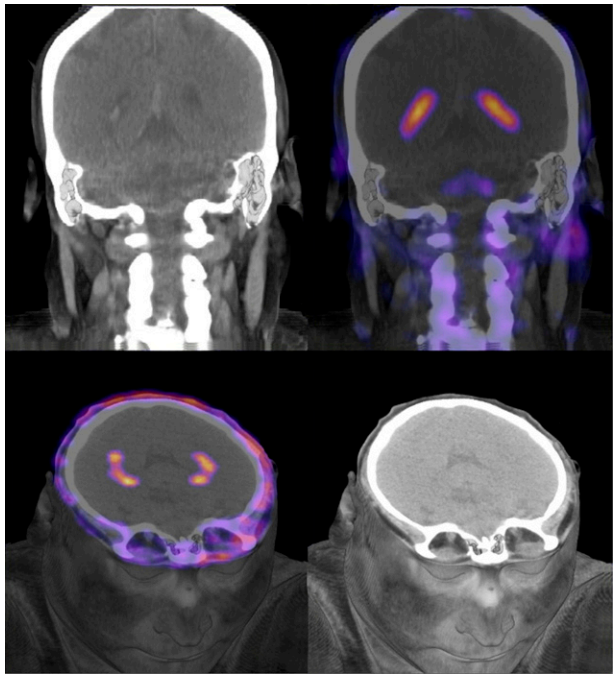

FIGURE 4. PET/CT (color) and CT (black and white) images showing normal uptake of ^{68}Ga-DOTA-E-[c(RGDfK)]$_2$ in choroid plexus at supratentorial ventricular system.

TABLE 2
Number of Disintegrations in Source Organs for Healthy Subjects Injected with ^{68}Ga-DOTA-E-[c(RGDfK)]$_2$

Source organ	Men (n = 3)	Women (n = 2)
Choroid plexus	5.43E−04 ± 7.51E−05	5.50E−04 ± 1.00E−05
Lower large intestine wall	2.97E−03 ± 7.02E−04	3.60E−03 ± 2.83E−04
Small intestine	7.05E−02 ± 1.63E−02	8.49E−02 ± 6.93E−03
Upper large intestine wall	2.54E−02 ± 5.88E−03	3.07E−02 ± 2.55E−03
Kidneys	3.28E−02 ± 6.26E−03	3.30E−02 ± 1.41E−02
Liver	8.95E−02 ± 1.78E−02	1.16E−01 ± 5.66E−03
Spleen	1.43E−02 ± 3.77E−03	1.41E−02 ± 3.82E−03
Thyroid	6.93E−04 ± 6.35E−05	6.70E−04 ± 1.56E−04
Urinary bladder contents (no voiding)	3.10E−01 ± 1.22E−01	2.98E−01 ± 1.11E−01
Urinary bladder contents (1-h voiding)	1.12E−01 ± 4.44E−02	1.27E−01 ± 6.04E−02
Urinary bladder contents (2.5-h voiding)	2.42E−01 ± 9.36E−02	2.74E−01 ± 9.10E−02
Remainder	8.09E−01 ± 1.08E−01	7.89E−01 ± 1.34E−01

Data are mean ± SD MBq·h/MBq.

TABLE 3
Absorbed and Effective Doses of ^{68}Ga-DOTA-E-[c(RGDfK)]$_2$ in Healthy Subjects Using Different Urinary Bladder Models

Target organ	Men (n = 3)			Women (n = 2)		
	No voiding	1-h voiding	2.5-h voiding	No voiding	1 h-voiding	2.5-h voiding
Adrenals	9.2 ± 0.6	9.1 ± 0.6	9.2 ± 0.6	12.0 ± 0.8	11.9 ± 0.8	12.0 ± 0.8
Brain	6.5 ± 0.5	6.5 ± 0.5	6.5 ± 0.5	8.2 ± 0.7	8.2 ± 0.7	8.2 ± 0.7
Breasts	6.6 ± 0.5	6.6 ± 0.5	6.6 ± 0.5	8.4 ± 0.9	8.4 ± 0.9	8.4 ± 0.9
Gallbladder wall	10.8 ± 0.7	10.7 ± 0.8	10.8 ± 0.8	14.1 ± 0.8	13.9 ± 0.9	14.1 ± 0.8
Lower large intestine wall	17.3 ± 0.6	14.7 ± 1.2	16.4 ± 1.3	22.0 ± 0.7	19.2 ± 0.1	21.6 ± 0.9
Small intestine	47.5 ± 5.2	46.5 ± 5.4	47.2 ± 5.3	64.3 ± 2.6	63.1 ± 2.4	64.1 ± 2.7
Stomach wall	8.9 ± 0.6	8.7 ± 0.6	8.8 ± 0.6	11.2 ± 0.9	11.1 ± 0.9	11.2 ± 0.9
Upper large intestine wall	36.2 ± 3.8	35.5 ± 3.9	36.0 ± 3.9	48.3 ± 1.6	47.4 ± 1.4	48.2 ± 1.7
Heart wall	8.0 ± 0.6	8.0 ± 0.6	8.0 ± 0.6	10.3 ± 1.1	10.3 ± 1.1	10.3 ± 1.1
Kidneys	53.9 ± 5.4	53.8 ± 5.3	53.9 ± 5.3	59.6 ± 16.5	59.4 ± 16.4	59.6 ± 16.5
Liver	26.6 ± 2.9	26.5 ± 2.9	26.5 ± 2.9	45.1 ± 1.6	45.0 ± 1.6	45.1 ± 1.6
Lungs	7.5 ± 0.6	7.5 ± 0.6	7.5 ± 0.6	9.7 ± 1.0	9.7 ± 1.0	9.7 ± 1.0
Muscle	8.4 ± 0.3	7.8 ± 0.6	8.2 ± 0.6	10.5 ± 0.6	9.8 ± 0.8	10.4 ± 0.6
Ovaries*	13.5 ± 0.2	11.1 ± 0.8	12.7 ± 1.0	17.3 ± 0.4	14.6 ± 0.3	17.0 ± 0.6
Pancreas	9.6 ± 0.6	9.5 ± 0.6	9.6 ± 0.6	12.2 ± 0.8	12.2 ± 0.9	12.2 ± 0.8
Red marrow	7.1 ± 0.3	6.7 ± 0.5	7.0 ± 0.5	8.8 ± 0.5	8.3 ± 0.6	8.7 ± 0.5
Osteogenic cells	10.7 ± 0.7	10.4 ± 0.8	10.6 ± 0.8	14.3 ± 1.4	14.1 ± 1.5	14.3 ± 1.4
Skin	6.7 ± 0.4	6.5 ± 0.5	6.7 ± 0.5	8.4 ± 0.8	8.1 ± 0.8	8.3 ± 0.8
Spleen	39.2 ± 5.5	39.1 ± 5.5	39.1 ± 5.5	47.1 ± 8.2	47.0 ± 8.2	47.1 ± 8.2
Testes	9.7 ± 0.1	8.0 ± 0.7	9.1 ± 0.8	0.0 ± 0.0	0.0 ± 0.0	0.0 ± 0.0
Thymus	7.3 ± 0.6	7.3 ± 0.6	7.3 ± 0.6	9.3 ± 1.0	9.3 ± 1.1	9.3 ± 1.1
Thyroid	16.5 ± 0.6	16.5 ± 0.6	16.5 ± 0.6	19.1 ± 2.5	19.1 ± 2.5	19.1 ± 2.5
Urinary bladder wall	363 ± 80	136 ± 30	285 ± 62	471 ± 121	206 ± 66	435 ± 140
Uterus*	18.1 ± 1.3	12.5 ± 1.1	16.2 ± 1.7	21.7 ± 1.7	16.1 ± 0.5	20.9 ± 2.0
Total body	9.8 ± 0.4	9.1 ± 0.7	9.6 ± 0.7	12.6 ± 0.5	11.9 ± 0.7	12.6 ± 0.5
Effective dose (μSv/MBq)	29.6 ± 3.7	17.4 ± 1.7	25.4 ± 3.3	38.5 ± 6.0	24.3 ± 3.1	36.6 ± 7.1

*Dosimetric calculations for men.
Data are mean ± SEM μGy/MBq.

could be associated with a higher in vivo affinity of the dimer molecule than of the monomer, since integrins are significantly expressed in choroid plexus epithelial cells and microglia (*39*).

A clinical protocol to evaluate the potential of ^{68}Ga-DOTA-E-[c(RGDfK)]$_2$ as a predictive biomarker of outcome in non–small cell lung cancer in patients treated with combined docetaxel and nintedanib is currently in progress at the National Institute of Cancer.

TABLE 4
Absorbed and Effective Doses to Critical Organs for RGD-Based Radiopharmaceuticals

Parameter	^{18}F-Galacto-RGD (*26*)	^{18}F-RGD-K5 (*27*)	^{18}F-FPPRGD2 (*29*)	^{68}Ga-NOTA-RGD (*28*)	^{68}Ga-DOTA-RGD$_2$ (this work)
Urinary bladder wall (μGy/MBq)	110 ± 20	103 ± 4	233 ± 118	208.6 ± 50.8	172 ± 100
Effective dose (μSv/MBq)	12.7 ± 2.2	15.1 ± 1	39.6 ± 18.1	23.3 ± 4.2	20.9 ± 5.1
Typical injected activity (MBq)	370	370	370	185	185
Estimated effective dose per scan (mSv)	4.7	5.6	14.7	4.3	3.9

Data are mean ± SD, acquired using 1-h bladder voiding model.

CONCLUSION

We have successfully estimated ^{68}Ga-DOTA-E-[c(RGDfK)]$_2$ human dosimetry in 5 healthy adults. These results provide the first, to our knowledge, human dosimetry data of a DOTA-conjugated RGD–dimeric peptide. The critical organ was urinary bladder wall, with a mean absorbed dose of 172 ± 31 μGy/MBq for the 1-h-voiding model. The mean effective dose, determined with the same model, was 20.85 ± 5.18 μSv/MBq. This radiopharmaceutical demonstrates a radiation dose comparable to other previously reported RGD-based radiopharmaceuticals labeled with ^{68}Ga and ^{18}F. In all cases, the urinary bladder wall had the highest dose among all organs and was deemed to be the critical organ; however, with diuretic agents and frequent bladder voiding, doses to the bladder wall and the whole body can be reduced. Therefore, ^{68}Ga-DOTA-E-[c(RGDfK)]$_2$ can safely be used for imaging integrin $\alpha_v\beta_3$ expression.

DISCLOSURE

The costs of publication of this article were defrayed in part by the payment of page charges. Therefore, and solely to indicate this fact, this article is hereby marked "advertisement" in accordance with 18 USC section 1734. This research was supported by CONACYT grant 179218 and International Atomic Energy Agency grant RC16467. No other potential conflict of interest relevant to this article was reported.

ACKNOWLEDGMENTS

We thank the staff of Unidad Radiofarmacia-Ciclotrón (Efraín Zamora-Romo, Juan C. Manrique-Arias, Fernando Trejo-Ballado, Gabriela Contreras-Castañón, Héctor M. Gama-Romero, Adolfo Zárate-Morales, and Armando Flores-Moreno) for assistance with radiopharmaceutical production and quality control. We also thank the nuclear medicine nurse, Gildardo Gamez-Maldonado, and the nuclear medicine technologists, José U. Martinez-Berry, Osvaldo Morales-Santillan, and Mario E. Romero-Piña, for their help in image acquisition.

REFERENCES

1. Velikyan I. Molecular imaging and radiotherapy: theranostics for personalized patient management. *Theranostics.* 2012;2:424–426.
2. Fass L. Imaging and cancer: a review. *Mol Oncol.* 2008;2:115–152.
3. Chen K, Conti PS. Target-specific delivery of peptide-based probes for PET imaging. *Adv Drug Deliv Rev.* 2010;62:1005–1022.
4. Banerjee SR, Pomper MG. Clinical applications of gallium-68. *Appl Radiat Isot.* 2013;76:2–13.
5. Kulkarni HR, Baum RP. Theranostics with Ga-68 somatostatin receptor PET/CT: monitoring response to peptide receptor radionuclide therapy. *PET Clin.* 2014;9:91–97.
6. Kulkarni HR, Baum RP. Patient selection for personalized peptide receptor radionuclide therapy using Ga-68 somatostatin receptor PET/CT. *PET Clin.* 2014;9:83–90.
7. Haug AR, Auernhammer CJ, Wängler B, et al. ^{68}Ga-DOTATATE PET/CT for the early prediction of response to somatostatin receptor–mediated radionuclide therapy in patients with well-differentiated neuroendocrine tumors. *J Nucl Med.* 2010;51:1349–1356.
8. Walker RC, Smith GT, Liu E, Moore B, Clanton J, Stabin M. Measured human dosimetry of ^{68}Ga-DOTATATE. *J Nucl Med.* 2013;54:855–860.
9. Lopez-Rodriguez V, Gaspar-Carcamo RE, Pedraza-Lopez M, et al. Preparation and preclinical evaluation of ^{66}Ga-DOTA-E[c(RGDfK)]$_2$ as a new theranostic radiopharmaceutical. *Nucl Med Biol.* 2015;42:109–114.
10. Knetsch PA, Petrik M, Rangger C, et al. [^{68}Ga]NS3-RGD and [^{68}Ga] Oxo-DO3A-RGD for imaging $\alpha_v\beta_3$ integrin expression: synthesis, evaluation, and comparison. *Nucl Med Biol.* 2013;40:65–72.
11. Stott Reynolds TJ, Schehr R, Liu D, et al. Characterization and evaluation of DOTA-conjugated bombesin/RGD-antagonists for prostate cancer tumor imaging and therapy. *Nucl Med Biol.* 2015;42:99–108.
12. Plow EF, Haas TA, Zhang L, et al. Ligand binding to integrins. *J Biol Chem.* 2000;275:21785–21788.
13. Brooks PC. Role of integrins in angiogenesis. *Eur J Cancer.* 1996;32A:2423–2429.
14. Dijkgraaf I, Yim CB, Franssen GM, et al. PET imaging of $\alpha_v\beta_3$ integrin expression in tumours with ^{68}Ga-labelled mono, di- and tetrameric RGD peptides. *Eur J Nucl Med Mol Imaging.* 2011;38:128–137.
15. Decristoforo C, Hernandez Gonzalez I, Carlsen J, et al. ^{68}Ga- and ^{111}In-labelled DOTA RGD peptides for imaging of $\alpha_v\beta_3$ integrin expression. *Eur J Nucl Med Mol Imaging.* 2008;35:1507–1515.
16. Knetsch PA, Petrik M, Griessinger CM, et al. [^{68}Ga]NODAGA-RGD for imaging αvβ3 integrin expression. *Eur J Nucl Med Mol Imaging.* 2011;38:1303–1312.
17. Chen X, Tohme M, Park R, et al. Micro-PET imaging of alphavbeta3-integrin expression with ^{18}F-labeled dimeric RGD peptide. *Mol Imaging.* 2004;3:96–104.
18. Ferro-Flores G, Ramírez F de M, Meléndez-Alafort L, et al. Peptides for in vivo target-specific cancer imaging. *Mini Rev Med Chem.* 2010;10:87–97.
19. Janssen M, Oyen WJ, Massuger LF, et al. Comparison of a monomeric and dimeric radiolabeled RGD-peptide for tumor targeting. *Cancer Biother Radiopharm.* 2002;17:641–646.
20. Liu S. Radiolabeled multimeric cyclic RGD peptides as integrin $\alpha_v\beta_3$ targeted radiotracers for tumor imaging. *Mol Pharm.* 2006;3:472–487.
21. Li ZB, Chen k, Chen X. ^{68}Ga-labeled multimeric RGD peptides for microPET imaging of integrin $\alpha_v\beta_3$ expression. *Eur J Nucl Med Mol Imaging.* 2008;35:1100–1108.
22. Fani M, Andre JP, Maecke HR. ^{68}Ga-PET: a powerful generator-based alternative to cyclotron-based PET radiopharmaceuticals. *Contrast Media Mol Imaging.* 2008;3:67–77.
23. Rösch F, Baum RP. Generator-based PET radiopharmaceuticals for molecular imaging of tumours: on the way to theranostics. *Dalton Trans.* 2011;40:6104–6111.
24. Rösch F. Past, present and future of ^{68}Ge/^{68}Ga generators. *Appl Radiat Isot.* 2013;76:24–30.
25. Decristoforo C, Pickett RD, Verbruggen A. Feasibility and availability of ^{68}Ga-labelled peptides. *Eur J Nucl Med Mol Imaging.* 2012;39(suppl):S31–S40.
26. Beer AJ, Haubner R, Wolf I, et al. PET-based human dosimetry of ^{18}F-galacto-RGD, a new radiotracer for imaging alpha$_v$beta$_3$ expression. *J Nucl Med.* 2006;47:763–769.
27. Doss M, Kolb HC, Zhang JJ, et al. Biodistribution and radiation dosimetry of the integrin marker ^{18}F-RGD-K5 determined from whole-body PET/CT in monkeys and humans. *J Nucl Med.* 2012;53:787–795.
28. Kim JH, Lee JS, Kang KW, et al. Whole-body distribution and radiation dosimetry of ^{68}Ga-NOTA-RGD, a positron emission tomography agent for angiogenesis imaging. *Cancer Biother Radiopharm.* 2012;27:65–71.
29. Mittra ES, Goris ML, Laguro AH, et al. Pilot pharmacokinetic and dosimetric studies of ^{18}F-FPPRGD2: a PET radiopharmaceutical agent for imaging $\alpha_v\beta_3$ integrin levels. *Radiology.* 2011;260:182–191.
30. Ortiz-Arzate Z, Santos-Cuevas CL, Ocampo-García BE, et al. Kit preparation and biokinetics in women of ^{99m}Tc-EDDA/HYNIC-E-[c(RGDfK)]$_2$ for breast cancer imaging. *Nucl Med Commun.* 2014;35:423–432.
31. Ma Q, Ji B, Jia B, et al. Differential diagnosis of solitary pulmonary nodules using ^{99m}Tc-3P4-RGD$_2$ scintigraphy. *Eur J Nucl Med Mol Imaging.* 2011;38:2145–2152.
32. Wan W, Guo N, Pan D, et al. First experience of ^{18}F-alfatide in lung cancer patients using a new lyophilized kit for rapid radiofluorination. *J Nucl Med.* 2013;54:691–698.
33. Stabin MG, Siegel JA. Physical models and dose factors for use in internal dose assessment. *Health Phys.* 2003;85:294–310.
34. Stabin MG, Sparks RB, Crowe E. OLINDA/EXM: the second-generation personal computer software for internal dose assessment in nuclear medicine. *J Nucl Med.* 2005;46:1023–1027.
35. Thomas SR, Stabin MG, Chen CT, Samaratunga RC. MIRD pamphlet no. 14 revised: a dynamic urinary bladder model for radiation dose calculations. Task Group of the MIRD Committee, Society of Nuclear Medicine. *J Nucl Med.* 1999;40(suppl):102S–123S.
36. Paulus W, Baur I, Schuppan D, et al. Characterization of integrin receptors in normal and neoplastic human brain. *Am J Pathol.* 1993;143:154–163.
37. Pinkstaff JK, Detterich J, Lynch G, et al. Integrin subunit gene expression is regionally differentiated in adult brain. *J Neurosci.* 1999;19:1541–1556.
38. Wu X, Reddy DS. Integrins as receptor targets for neurological disorders. *Pharmacol Ther.* 2012;134:68–81.
39. Engelhardt B, Sorokin L. The blood-brain and the blood-cerebrospinal fluid barriers: function and dysfunction. *Semin Immunopathol.* 2009;31:497–511.

The Journal of NUCLEAR MEDICINE

PET-Based Human Dosimetry of the Dimeric $\alpha_v\beta_3$ Integrin Ligand ^{68}Ga-DOTA-E-[c(RGDfK)]$_2$, a Potential Tracer for Imaging Tumor Angiogenesis

Victoria López-Rodríguez, Carlos Galindo-Sarco, Francisco O. García-Pérez, Guillermina Ferro-Flores, Oscar Arrieta and Miguel A. Ávila-Rodríguez

J Nucl Med. 2016;57:404-409.
Published online: November 19, 2015.
Doi: 10.2967/jnumed.115.161653

The Journal of Nuclear Medicine is published monthly.
SNMMI | Society of Nuclear Medicine and Molecular Imaging
1850 Samuel Morse Drive, Reston, VA 20190.
(Print ISSN: 0161-5505, Online ISSN: 2159-662X)

SNMMI SOCIETY OF NUCLEAR MEDICINE AND MOLECULAR IMAGING